

# Scholar Journal of Applied Sciences and Research

## Development of Air Plasma Thermal Spray Coating for Thermal Barrier Coating and Oxidation Resistance Applications on Ni-Base Super Alloys

Ahmed KF<sup>1\*</sup>  
Shoeib MA<sup>2</sup>

<sup>1</sup>Arab Institute for Advanced Technology (A.I.A.T), AOI, Egypt

<sup>2</sup>Head Corrosion Control and Surface protection, CMRDI, Egypt

### Abstract

Aerospace gas turbine engines are now designed such that the heat resistant super alloys operate at temperature very close to their melting, so current strategies for performance improvement are centered on thermal barrier coatings. Lower thermal conductivities lead to temperature reductions at the substrate/bond coat interface which slows the rate of the thermally induced failure mechanisms. Alternatively, lower thermal conductivity TBC layers might allow designers to reduce the TBC thickness there by decreasing the significant centrifugal load that the mass of the TBC imposes on the rotating turbine engine components. One approach to improve TBC system is to optimize the pore morphologies to reduce the thermal conductivity while still retaining high in-plane compliance. The second approach to improve TBC system performance is to optimize the surface microstructure, surface densification, phase structures mechanical characteristic, chemical structure, and thermo-physical properties.

The focus of this work is to study the influence of Al PO<sub>4</sub> (and laser)-sealed ZrO<sub>2</sub>-MgO coatings on thermal barrier coating system comprised of zirconia stabilized with magnesia top coat to predict the best improvement of TBC system and to optimize the surface microstructure, surface densification, phase structures, mechanical characteristic, chemical structure, and thermo-physical properties as well as their properties with those obtained using reference techniques. Thermal expansion studies were used to study the high temperature stability of the different coatings (reference and modified coatings) structures. As low thermal conductivity is one of the most important features of TBC, thermal diffusivity and specific heat measurements were carried out. Also, the mechanical measurements (e.g. micro-hardness, tensile bond strength, young's modulus), phase analyses using XRD and chemical analysis using electron dispersive X-ray (EDX) for elemental analysis in scanning microscopy studies.

**Key words:** Thermal barrier coating, air plasma spray, heat treatment, thermal expansion coefficient, thermal conductivity, zirconia stabilized with magnesia, nickel aluminum, laser sealed zirconia coatings and laser sealed ZrO<sub>2</sub>-MgO coatings.

### Introduction

Plasma is quasi-neutral multi particles system which characterized by gaseous or fluid mixtures. It consists of electrons, positively charged ions and neutral gas, atoms, molecules or radicals [1]. Mono-atomic gases require only to be ionized to enter the plasma state, while bimolecular gases must be first dissociated before ionization, thus need larger energy to enter plasma state. Small quantities of hydrogen (or helium)

### Article Information

**Article Type:** Research

**Article Number:** SJASR120

**Received Date:** 05 May, 2018

**Accepted Date:** 22 May, 2018

**Published Date:** 04 June, 2018

**\*Corresponding author:** Dr. Ahmed KF, Arab Institute for Advanced Technology (A.I.A.T), AOI, Egypt. Email: [khalidfareed330@yahoo.com](mailto:khalidfareed330@yahoo.com)

**Citation:** Ahmed KF, Shoeib MA (2018) Development of Air Plasma Thermal Spray Coating for Thermal Barrier Coating and Oxidation Resistance Applications on Ni-Base Super Alloys. Sch J Appl Sci Res. Vol: 1, Issu: 3 (20-35).

**Copyright:** © 2018 Ahmed KF, et al. This is an open-access article distributed under the terms of the Creative Commons Attribution License, which permits unrestricted use, distribution, and reproduction in any medium, provided the original author and source are credited.

added as a secondary gas to argon lead to increase of both plasma enthalpy and heat transfer rates from the plasma to the powder particles [2].

Thermal barrier coating: (TBC) are often applied to metallic super alloys to extend the temperature regime in which a component can operate [3,4]. A typical application is in gas turbine engines, where thin TBC have been utilized for many years. Prime requirements for the ceramic thermal barrier coatings are low thermal conductivity and thermal expansion compatible with the metallic substrate. The most suitable appears to be the magnesia-zirconia system which has already become established as plasma spray thermal barrier coatings in high temperature aero engine application. Magnesia-zirconia are nevertheless considered the best prospective starting materials for industrial gas turbine, TBC and the test programmed was therefore concentrated on modifying zirconia-stabilized with magnesia to give optimum properties. Zirconia-stabilized with magnesia coating have been used in aircraft gas turbines as thermal barriers in combustor cans for several years. They have more recently been utilized on high pressure nozzle guide vane plat forms and there is much interest in coating the pressure surfaces of turbine blades. Plasma sprayed magnesia stabilized with zirconia coatings consist of porous phase material attached to a substrate by an intermediate bond coat. The porous nature of the coating greatly enhances thermal and crack resistance.

The modern TBC are required to not only limit heat transfer through the coating but to also protect engine components from oxidation and hot corrosion. No single coating composition appears able to satisfy these multifunctional requirements. Research in the last 20 years has led to a preferred coating system consisting of more than one separate layer to achieve long term effectiveness in the high temperature [5], oxidative and corrosive use environment for which they are intended to function.

## Experimental Procedures

### Plasma apparatus and process description

PLASMA-TECHNIK AG M-1000 apparatus is used for plasma spraying has improved and developed plasma torches and auxiliary equipment for the spraying of aerospace components. It comprises: power source (PT-800), control unit (PT-M1000), plasma torch- (F4), powder feed unit (TWIN- 10), water cooler system (T-500) and holding device for the work piece, in addition to dust separator (MK-9) and wet separator (NA-100). Figure 1 shows the schematic diagram of the PLASMA-TECHNIK AG M- 1000 apparatus.

A path is pre-ionized for the direct current arc from the cathode to the anode using high frequency (HF) sparking. The direct current arc energized from the power source ionizes the gas flowing through the torch (ionization = electron excitation). The gas flow drives the arc contact point in the anode nozzle forward and the arc stabilizes. Argon gas is used for arc initiation (easily ionized) and following stabilization, an auxiliary gas is normally added, usually  $H_2$ . Gases, such as  $H_2$  or  $N_2$  (with two atoms) dissociate at high temperatures before ionizing. Therefore, they exhibit a

higher energy (for a certain temperature) than gases such as Ar or He (single atoms). The mixture of electrons, ions and neutral gas particles is the plasma i.e. a gas with an extremely high temperature (between 10000 and 30000 k) and heat capacity. The increase in temperature causes the plasma to exit from the anode nozzle with a high velocity. The spray powder is introduced into the hot, fast plasma using an injector and the particles are heated and accelerated. The powder particles become molten and impact on the surface to be coated with a high kinetic energy where they form a laminar coating. Plasma spray coating is produced by successive impacts of accelerated particles in a molten state on the substrate (i.e. a single specimen was cut from flat Ni-super alloy sheet (NiCr20TiAl of DIN designation number is 2.4631), with dimensions  $40 \times 20 \times 1.4$  mm) or previously deposited layers, the next particle impacting on an already completely solidified one.

### Advanced processing approaches for producing TBC of high quality performance

**Pretreatment procedure of substrate:** GRID-BLASTING is generally used as a pretreatment method of substrate to increase the average surface roughness.

An effective pre-treating way is experientially known that by NTA (Negative Transferred Arc) in which a reversed transferred arc is generated between a plasma - gun nozzle and a substrate by putting an electric-voltage between them and then with applying LPPS (Low pressure plasma spray) Figure 2, by using a  $H_2$  mixed Ar plasma jet. And they showed these erosions were formed by a melting of surface materials due to a high concentration of electric currents at the density of about  $10^8$  A/cm<sup>2</sup> into microscopic cathode arc spots where an arc discharge was taking place [6-12]. The surfaces of Ni-base super alloy substrates were cleaned, and numerous small spikes were formed by the erosion process of an arc discharge (the surface roughening was found to be caused by the formation of numerous microscopic cathode spots all over the surface). Table 1 shows NTA process parameter on the surface of specimens (Ni-base super alloy substrate).

**Air plasma thermal spray coating and post-spray treatment procedure of substrate:** First, Ni-5wt % Al (AMDRY 956) powder can be applied to form the suitable bond coat of high hot corrosion resistant and oxidation resistant coating of 0.05 mm as a minimum thickness on Ni-base super alloy surface (substrate). and by introducing an intermediate layer composed of ceramic with alloy (i.e. combination of 65wt %  $ZrO_2$ -MgO) (AMDRY 333) and 35wt% of Ni-Al (AMDRY 956) which they are corresponding to AMDRY 341) that air plasma thermally sprayed on the under layer bond coat to create compositions that possess the specific properties required for a particular new proprietary application and then the top coat,  $ZrO_2$ -20wt % MgO (AMDRY 333) of 0.3 mm to 0.8 mm thickness have been deposited by air plasma spraying in method upon their surface.

The characteristics of sprayed and their acceptance criteria for coatings were given in Table 2. The key parameters controlling the thermo-mechanical properties of plasma sprayed (Direct Current plasma spraying) are the

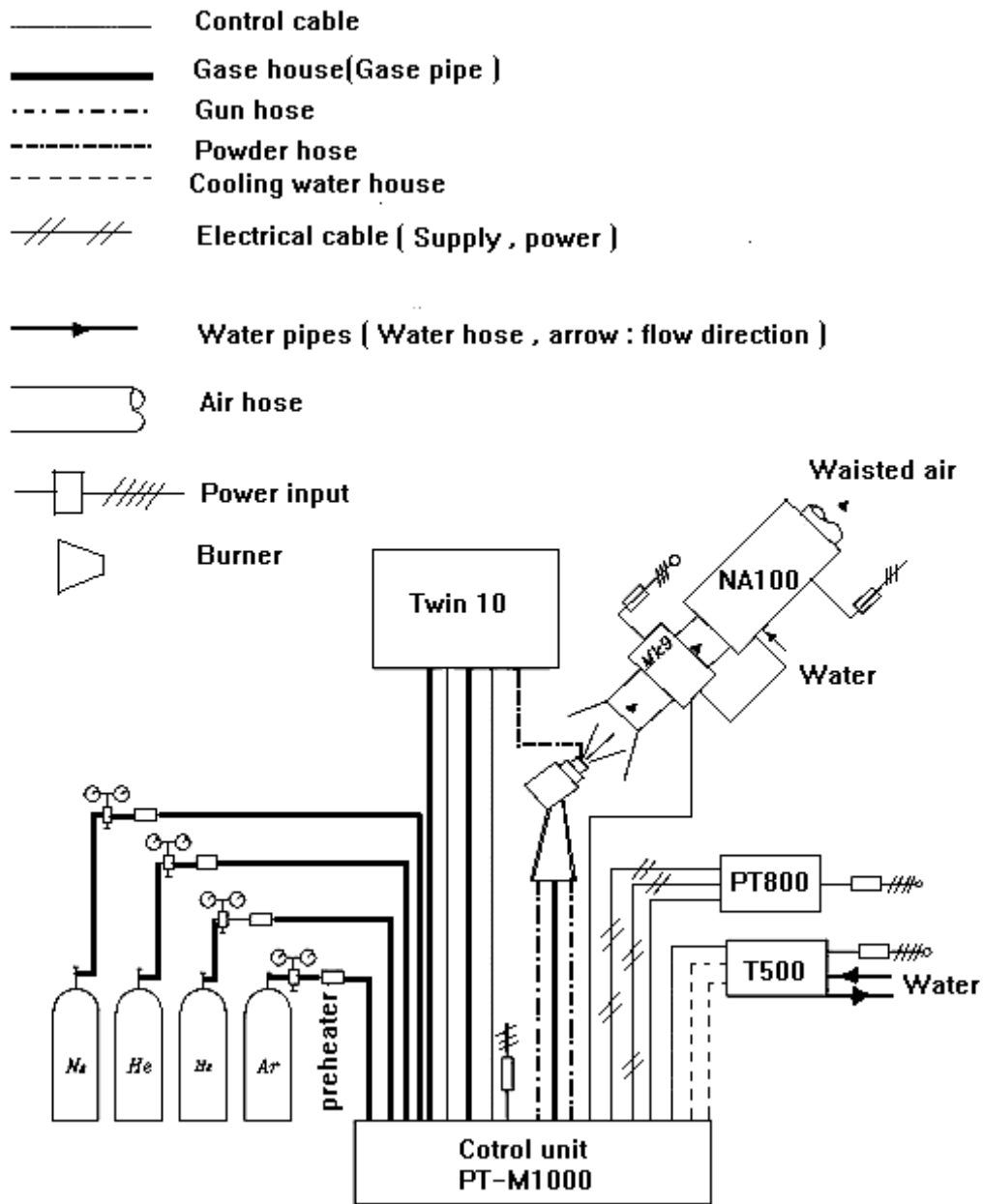


Figure 1: Systematic diagram of (Plasma-Technique AG M-1000).

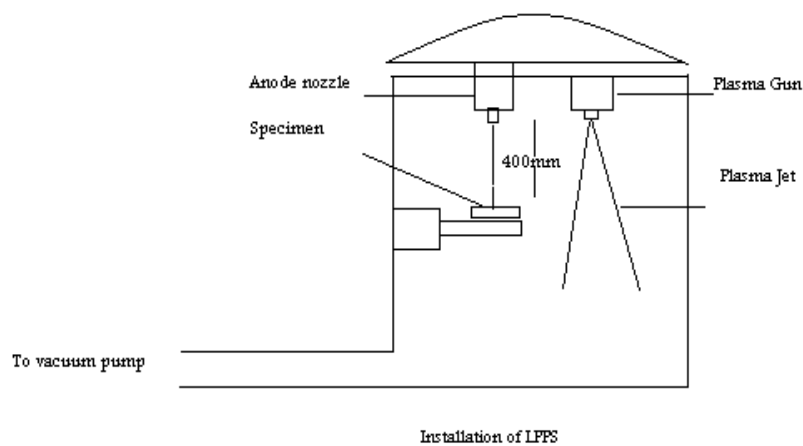


Figure 2: Installation of LPPS for the NTA process applied on substrate.

**Table 1:** The NTA process parameters applied on Ni-super alloy substrate corresponding to tensile bond strength.

Plasma generating gas	Distance between gun and specimen (mm)	Duration of NTA processing (Sec)	NTA Electric current (A)	Surface roughness ( $\mu$ .m)	Improved tensile bond strength (M Pa)
Ar. + 15 volume % H <sub>2</sub>	500	0.1 - 2	35A	20 $\pm$ 2	65

**Table 2:** Characteristics of air plasma thermal spraying and their acceptance Criteria.

Powder Characteristics			Coating characteristics					
Spray Powder	Grain Size ( $\mu$ .m)	Allowed Thickness (mm.)	Micro-hardness (HV <sub>3</sub> )	Tensile bond strength (M. Pa)	Porosity (%)	Un-bonded (Separate) Particle (%)	Density (g/cc)	Operation Temperature (°C)
AMDRY 956 bond coat over substrate	45 ~ 90	0.05 ~ 1	Min 180	Min 35	Max 2, diameter $\varnothing$ m<30 $\mu$ m	Max 15, diameter $\varnothing$ m<15 $\mu$ . M	Min 7.43	Max 870
AMDRY 341 intermediate coat) over bond coat	10 ~ 90	0.05 ~ 1	190	30	10 Diameter $\varnothing$ m < 30 $\mu$ m	15 diameter $\varnothing$ m < 60 $\mu$ m	Min 5.4	Max 900
AMDRY 333 (Top Coat)	10 ~ 45	0.1 ~ 0.5	Min 200	Min 22	Max 15, diameter $\varnothing$ m<30 $\mu$ m	Max 15, diameter $\varnothing$ m<60 $\mu$ m	Min 4.28	Max 1000

heat and momentum transfers between the plasma jets and the injected particles. These, beside the particles size and plasma gas nature, depends strongly on the plasma isotherms lengths and diameters which in turn controlled by nozzle. Table 3 show the different spray parameters of control unit PT-M 1000, powder feed (TWIN-10) and plasma torch (F4). All the coatings were sprayed using commercial feed stock powders. Most of the coating modification procedures were undergoing post-treatments as heat treatment and / or chemical treatment [13,14].

### Heat treatment

**Furnace treatment:** A heat treatment is applied to sinter the coating, previously detached from the substrate. Since, an electric current conduction associated treatment process, or a furnace treatment process used to enhance the adhesion of the bond coatings deposited on to the turbine blades (Ni-super alloy substrate), increase coating density and its elastic modulus.

**Laser (sealing) treatment:** Laser (sealing) has been used for the improvement of plasma- sprayed TBC properties by reducing surface roughness, micro-structural heterogeneities (such as un-melted / partially melted powder particles, pores, cavities and voids) within the lower region of the melted layer and sealing open porosity to increase micro hardness, erosion and abrasion resistance.

Coatings were laser-glazed using quanta-Ray from flash lamp- pumped Q-switched oscillator - amplifier Nd-YAG (Neodymium-doped Yttrium Aluminum Garnet) laser rod system. The width of the laser beam was 10 mm at the focused area which was at the distance of 1000 mm from the mirror. Laser glazing parameters were optimized for studied thick- thermal barrier, coating using pulsed laser beam; the parameters are presented in Table 4. In the optimization stage the predetermined melting depth of the coating surface was reached without causing coating spoliations. The Q-switched Nd-YAG laser has various forms of material processing because they can be focused to a very small spot to give high- power pulsed versions for studies of inertial confinement fusion.

### Chemical treatment

**Phosphate (sealing) treatment:** The zirconia stabilized with Magnesia (ZrO<sub>2</sub>-20wt % MgO) coating were sealed with Al (OH)<sub>3</sub> -(85%) H<sub>3</sub>PO<sub>4</sub> solution diluted to 20 by wt % of de-ionized water. The ratio of Al (OH)<sub>3</sub>: (85%) H<sub>3</sub>PO<sub>4</sub> was 1:4.2 by weight. The solution was mixed and slightly heated with a magnetic stirrer until it became clear. ZrO<sub>2</sub>-MgO coating was sealed with aluminum phosphate sealing. Sealant was spread onto the coating surface and it instantly started to infiltrate into the coating cracks and pores. After that the specimens were placed in a furnace for heat treatment. The heat treatment was performed at 300°C for 4 hours.

### Surface investigation

**Metallographic test and phase analysis procedures:** A sample on which a deposit has been applied, is cut perpendicular to its coated surface, then encapsulated and polished, micrographic cross-section is initially, observed overall magnified by 75 to 200 times. Area considered as representative of the sample are re-examined with a magnification of 500- 2000 times. Cross-sections were made in the plane perpendicular to the treated surface using an optical microscope with different magnification. The metallographic examinations of the coat have been investigated by using scanning electron microscopic examinations (SEM).

The material of a flat sheet metal specimen has the following dimensions 40 mm  $\times$  20 mm  $\times$  1.4 mm after having coated the specimen thickness surface, make a cross- section perpendicular to the scanning direction. The coating thickness to be applied (measured with a flat anvil micrometer) is mentioned on the drawing or any additional document, with a minimum thickness of 0.05 mm for the bond coat and that of 0.3 mm for the top coat.

X- ray diffraction (XRD) was used in phase identification and quantitative phase analysis studies. The quantitative identification of the base material has analyzed by using X-ray diffraction (XRD) and spectrum technique electron diffraction X-ray(EDX). The phase compositions of the coating were identified with X-ray diffract-meter of type,

**Table 3-A:** Spray parameters of powder feeder; plasma gas and control unit: (A) Powder feeder (TWIN-10) and plasma torch (Gun) Parameters.

Powder Number	Carrier gas (Ar)		Injector diameter Ø (mm)	Injector distance (mm)	Injector support (angle) (°)	Gun type	Spraying distance (mm)	Motor digital display Disc (rpm)	Spray rate (gm./min)
	Pressure (Bar)	Flow rate (L/min)							
AMDRY 956	2.5	1.7	1.5	6	90°	F4	125-130	15-20	25-35
AMDRY 341	2.5	2.5	1.8	5.5	90°	F4	100	20	30
AMDRY 333	2.5	2.5	1.8	8	90°	F4	90	20	25-28

**Note:** Adjust the Motor digital display, Disc (rpm) as required to obtain indicated spray rate.

**Table 3-B:** Spray parameters of powder feeder; plasma gas and control unit: (B) Control unit parameters.

Powder Number	Plasma gas flow rate (L/min)		Plasma gas pressure		Current (A)	Voltage (V)
	Primary Ar	Secondary H <sub>2</sub>	Primary Ar	Secondary H <sub>2</sub>		
AMDRY 956	47	9.5	2.5	2.5	450	65 - 68
AMDRY 341	47	13	2.5	2.5	630	70 - 72
AMDRY 333	47	13	2.5	2.5	630	70 - 72

**Note:** Adjust flow as required to obtain indicated voltage, voltage depend on flow rate and the type of the torch (gun).

(Siemens D500. Karlsruhe, Germany), uses Cu K $\alpha$  radiation with scan step of 0.02° and step time of 1.2 sec. Erosion tests were performed with a centrifugal accelerator using 250 gm Al<sub>2</sub>O<sub>3</sub> erosive, particle size of 45-90  $\mu$ m. The specimens were attached to the centrifuge rim with fixed angle. The average particle velocity was 50 m/s.

### Mechanical analysis procedures

**Micro-hardness testing:** The micro-hardness of the treated and untreated surface was determined using identical micro-hardness tester using micro-vickers machine with 30 gm load for 15 second. The hardness after plasma thermal spraying process at different zones was determined for surface- treated specimens. A specimen without plasma thermal spray coating was used as reference substrate. The Vickers micro-hardness test is used for coatings measurements under load 3N (e.g. HV<sub>3</sub> is the Vickers number for 3N load) describe the micro hardness of individual lamellae. The commercially available testers flow the normal procedures (e.g. ASTM E-384- 73 standard).

**Tensile bonding test:** The tensile bond strength measurement takes place by using ASTM 633- 96 (or DIN 50160) standards. Bonding of sprayed coating is measured by using a traction machine. The installation must allow carrying out the test perpendicular to the coated surface, and the load application rate is constant, between 0.8 and 1.2 mm/ min. Bond strength value or stress to rupture is the ratio between the rupture load and the bonding surface, this is expressed in Mega-Pascal (M Pa). For coating with a single layer, thicknesses required are 150  $\mu$ m to 200  $\mu$ m.

Surface preparation conditions for receiving the coating must be identical to those applied on the item. The surface to be glued must be degreased, sand blasted and dusted. Gluing process takes place by use FM 1000 epoxy polyamide film glue (American Cyanamid) or equivalent.

**Friction and wear resistance measurement:** The determination of the coefficient of dynamic friction can be found by using of a set - up shown in figure 3 and applying of the following equation:

$$\mu_f = \frac{F_{(T)}}{F_{(N)}}$$

Where F<sub>(T)</sub> is the force of friction and F<sub>(N)</sub> is the force of pressing.

There are three different kinds of friction are friction at sliding, rotation, and rolling.

The basic wear mechanism of thermally sprayed coating has been tested mainly for the adhesive, abrasive, and erosive wear. Oxide coating sprayed using the APS techniques have been tested for protection against two-body abrasion. The zirconia coating sprayed by use of the APS techniques were submitted to abrasion against silicon carbide (Si C) paper of grade 320. The abrasion test conducted under a load of 23 kg. The hardness and abrasion resistance are drops if the powder feed rate is too high. This phenomenon is due to the presence of un-melted grains, that increase with the powder feed rate. These grains are easily removed in abrasion conditions.

**Corrosion resistance test:** Linear polarization and Potentiodynamic (potential dynamic) techniques were used to determine the corrosion rate as well as the corrosion behavior of specimens. These experiments were carried out using AUTOLAP PGSTAT 30 which shown in Figure 4. Accelerated corrosion experiments were carried out using: linear polarization technique by subjecting the working electrode to a potential range of 25mv below and above corrosion potential (E<sub>corr</sub>) at a scan rate of 0.1mv/sec. The corrosion current (I<sub>corr</sub>) and hence the corrosion rate (CR) can be related to the slope of the potential vs. current plot ( $\Delta E/\Delta I$ ), known as the polarization resistance (R<sub>p</sub>) and simply by I<sub>corr</sub> = B/R<sub>p</sub>, where B is a constant. Potentiodynamic polarization tests were conducted by sweeping the potential with scan rate of 1mV/s from -100 mV below E<sub>corr</sub> to 1000mV above E<sub>corr</sub>. This test was performed to study the corrosion behavior of specimens before and after plasma thermal spray technique.

### Physical and thermo physical analysis procedures

**Thermal expansion and Thermal cycling test:** Thermal expansion studies and the determination of thermal expansion coefficient, TEC, were carried out by dilatometer (Adamel lhomargy SAS, model DI- 24, France) in air at a temperature of 50- 1300°C. The temperature

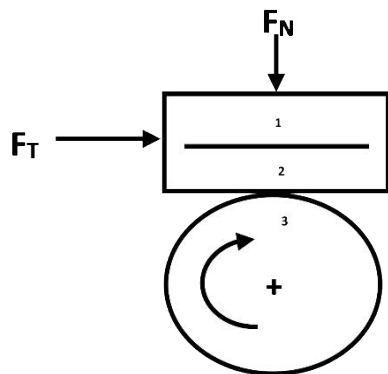


**Figure 3:** The set-up to determine the coefficient of dynamic friction, 1-substrate, 2-coating, 3-rotating wheel, FN- Load and FT-Friction.

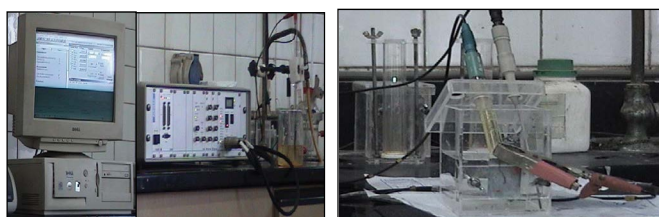


**Figure 4:** Photograph of AUTOLAP PGSTAT 30 and corrosion cell.

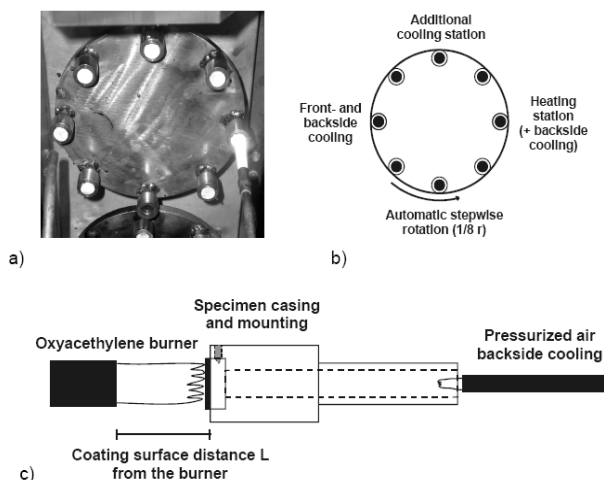


**Figure 5:** Illustration of the thermal cycling device, a- photo of the upper specimen holder during the test, b- position of heating and cooling stations and c- side view of the specimen mounting.

ramping or varied from 5°C/min to 10°C/min and dwell time at maximum temperature from 5 minutes to 5 hours.

Thermal barrier coatings have performed creditable in thermal cycle tests. Coating failure by thermal cycles depends on the applied stress on it and the strength of the substrate adhesion and interlinking to the coating. Thermal cycling resistance of the modified TBC was studied in a thermal cycling facility shown in Figure 5 which illustrates the positions of the heating and cooling station of each rotation of one holder. At the heating station the specimen was heated up by an oxy-acetylene burner. A maximum temperature of

the coatings, 1200°C, was fixed with the burner distance (L) from the coating surface and with the burner gas flow rates. At the primary cooling station, the specimens were cooled from the front and back by pressurized air. At the top position of the holder there was an optional front side cooling station, which was used only in part of the tests. The test parameters of each series are presented in Table 5. The additional cooling was used only after certain numbers of cycle. Coating was rated to be a failure by visual inspection when 10% of the coating was peeled off. The coating surface temperatures were measured by pyrometer based thermal camera (Therma Cam PM 595 FLIR systems, Portland, OR, USA).

**Porosity and pore distribution:** The normal procedure for coating materials (e.g. American B 328- 73) seems to be quite well adapted to test thermal sprayed coatings.

Porosity was tested with commercially available mercury intrusion porosity meter [14]. The method consists of evacuating the sample and immersing in mercury at low pressure, mercury is then pressurized, and the series of pressures and corresponding volumes of intruded mercury is determined. This method enables the total porosity and pore distribution to be determined. The porosity influences many mechanical and physical properties of the coatings. Finally, the determination of the porosity in many cases enables the prediction of other properties of the sprayed material.

**Thermal diffusivity test:** Thermal diffusivity, ( $\alpha$ ) measured out with laser flash apparatus Theta (Theta Industries Inc., Port Washington, NY, USA) in vacuum (0.01 pa). Measurements were performed at many different temperatures in the temperature range of 27°C up to 1200°C. Measurements were reported five times at each temperature for statistical reasons. Prior to evaluating the thermal diffusivity, to make the sample surfaces opaque, thin layers of colloidal graphite were painted on both the front and the rear faces.

**Specific heat test:** Specific heat, Cp, measurements were performed by a differential scanning calorimeter DSC404C (Netzsch- Geratebau GmbH, Selb, Germany). The scanning rate was 15°C/min at the temperature range of 27°C up to 1200°C. Measurements were carried out in air and in argon atmospheres using either alumina or platinum crucibles. Weight of the free-standing coating specimen was approximately 100 mg. for each sample three consequent measurements cycles were performed to lower the statistical error of the measurements.

**Apparent density test:** The measurements of apparent density and flow-ability was carried out by methods described e.g. by ASTM standards B 329-76 [15] and B 213-83 [16] receptively. The density measurement consists of weighing the sample of powder which fills the calibrated volume cup (of 25 cm<sup>3</sup>) and flow ability determination consists of measuring time necessary to flow out the 50-gm. sample of powder from the funnel of the calibrated orifice (2.54 mm).

**Thermal conductivity calculation:** Thermal

**Table 4:** Quanta-ray parameters of laser (sealing) for micro-structure modification and improve porosity.

Laser source	Q-switched Nd- YAG
Mode of the laser work	(single pulse wave)
Radiation wave length (nm)	1064
Pumping method	Optical Flash Lamp
Spatial profile of the beam	Linear polarized
Laser power output (watt)	1
Beam diameter (mm)	10
Distance between the last lens and the treated surface (mm)	1000
Cooling system	Compressed air
Linear scan velocity mm / sec	5

**Table 5:** The suitable parameters for the thermal cycling test of TBC.

Parameter	Test
Coating burner distance (mm)	50
Coating maximum temperature (°C)	1200
Coating minimum temperature (°C)	250 ± 50
Heating time (sec)	20
Total cycle number	500

conductivity,  $\lambda$ , was calculated using the following equation:

$$\lambda = C_p \times \alpha \times \rho.$$

Thermal conductivity values were calculated at 100°C intervals at a temperature range from 27°C to 1200°C, for these temperature points the diffusivity data was interpolated from the original data [17].

**Young's modulus measurement procedure (ultrasonic test):** A free-standing plate (or bar) is prepared by spraying a coating of low TEC (e.g. zirconia stabilized magnesia or nickel-aluminum) on a previously heated metal mandrel of high TEC (e.g. aluminum), the coating is detached after cooling down without any effort.

The young's modulus can determine using dynamic methods. Ultrasonic methods are especially well adapted to test small free-standing plates [18]. The method consists of generating vibration in the specimen (a small free-standing plate) and determining it's frequently by using the modern ultrasonic tester of elastic modulus (Reproduced by premising of J.W. lemmens-Elektronika NV, Leuven, Belgium). The frequency depends on the shape, density and young's modulus, which can be found by suitable mathematical treatment.

## Results and Discussion

### Microstructure and phase analysis investigation

**Microstructure and phase analysis investigation for heat treated coatings:** Polycrystalline bodies have complicated microstructures which consist of grains, grain boundaries and pores. Thus, micro structure parameters which control the physical properties of sintered bodies are grain size, grain boundary thickness, size and number of pores, and their geometric distributions. Sintering additives (e.g. MgO) in sintering materials tend to segregate on the surface or along grain boundaries. Thus, the amount and distribution of second phases are also important factors which determine the physical properties of the sintered bodies.

Total porosity, determined by image analysis, of the as-

sprayed coatings, was decreased by 60-70% due to high temperature exposure. The porosity and the mechanical properties results were presented in Table 6. The effect of sintering on ZrO<sub>2</sub>-MgO top coating is illustrated in SEM micrographs, Figure 6, by remaining strings of fine pores and closed cracks, at splat boundaries. A continuous interface is observed between the ZrO<sub>2</sub> particle and matrix and there appears to be no separation and voids, which indicates excellent wetting and adhesion between the two constituents. The total porosity of ZrO<sub>2</sub>-MgO top coat of the TBC systems, determined by image analysis of the as sprayed coating was decreased by 60%. But the open porosity of ZrO<sub>2</sub>-MgO top coat, determined by commercially available mercury intrusion porosimetry or Archimedes' methods, remained fairly content before and after the heat treatment. Sintering shrinkage seemingly did not affect the open porosity, and mercury porosimetry results showed no clear evidence of reduction of the very fine pores or micro-cracks.

Porosity of the heated ZrO<sub>2</sub>-MgO coatings was difficult to measure and interpret, because the present of traces of m-ZrO<sub>2</sub> made the structure slightly brittle. Moreover, the MgO precipitates, which were dark spots in optical micrographs, complicated the image analysis.

**Microstructure investigation for Aluminum phosphate sealed ZrO<sub>2</sub>-MgO coatings:** The microstructure of sealed coatings was investigated by SEM to understand the bonding and strengthening mechanism related to phosphate sealing. The penetration of Aluminum phosphate sealed into the (zirconia stabilized with magnesia top coat) coatings near the surface is illustrated by SEM micrographs in Figure 7. EDX results of the Aluminum phosphate sealed coatings are presented in Table 7 and Figure 8. The as-sprayed coating shows the Aluminum rich areas were in the coating micro-cracks.

It found that, the strengthening in phosphate sealing result from two different mechanisms, chemical bonding may be due to chemical reaction bonds the coating material and the sealant or/and adhesive binding may be due to the formation of condensed aluminum phosphate in the structural defects

**Table 6:** The effect of the furnace treatment processes on the coating performance of the TBC.

Sprayed Material Type	Furnace treatment			Property improved							
	Temperature (°C)	Time (h)	Atmosphere	Porosity (%)		Density (gm./cc)		Young's Modulus (G Pa)		Tensile bond strength (M Pa)	
				Before	After	Before	After	Before	After	Before	After
Ni-5wt% Al bond coat sprayed on Ni-substrate	1150	2	Vacuum	----	----	7.50	7.51	190	200	65	80
	800	24									
65 wt% ZrO <sub>2</sub> MgO plus 35wt% Ni- Al intermediate coat sprayed on the bond coat	800	4	Air	----	----	5.51	5.66	91	135	37	54
ZrO <sub>2</sub> -20wt % MgO top coat sprayed on the intermediate	1150	4	Air	9.8	5.8	4.23	4.48	62	69	33	48

**Table 7:** EDX result of Al PO<sub>4</sub> sealed ZrO<sub>2</sub>-MgO coatings.

Position of analysis	Compound (w.t %)		Element (w. t %)							
	ZrO <sub>2</sub>	Mg O	Al PO <sub>4</sub>	Zr P <sub>2</sub> O <sub>7</sub>	Al <sub>2</sub> O <sub>3</sub>	Zr	Mg	Al	P	O
Outer the coating cracks	78.2	21.8	-	-	-	60.9	13.1		-	25.9
Inner the coating cracks	77.9	21.8	0.05	0.12	0.13	60.7	9.3	2	1.8	26.2

**Table 8:** The quantitative XRD phase analysis results for aluminum phosphate sealed ZrO<sub>2</sub>-MgO top coat.

Position of analysis	m-ZrO <sub>2</sub> (w.t) %	t-ZrO <sub>2</sub> (w.t) %	c-Mg O (w.t) %	ZrP <sub>2</sub> O <sub>4</sub> (w.t) %	Al <sub>2</sub> O <sub>3</sub> (w.t) %
XRD analysis at outer the coating cracks	0.08	78.12	21.8	—	—
XRD analysis at inner the coating cracks	0.08	77.87	21.8	0.12	0.13

of the coating [19,20]. But phosphate sealant, penetrated the inter-lamellar crack in ZrO<sub>2</sub>-MgO coating, is present in SEM micrograph. The high magnification SEM images showed no visible reaction layer in the coating/sealant interface, so it can be assumed that here the bonding is based mainly on the adhesive binding mechanism. Since in our earlier study [21], we showed that, in the case of ortho-phosphoric acid sealed ZrO<sub>2</sub>-MgO coating, the sealant also amorphous form but the strengthening in ortho-phosphoric sealing is a result from chemical bonding between the coating material and the sealant. And from the XRD analysis of the phosphate sealed coatings which was made after removing only the extra sealant from the surface, the result identified clear zirconium phosphate (ZrP<sub>2</sub>O<sub>7</sub>) peaks in the ZrO<sub>2</sub>-MgO coatings, Table 8 and Figure 9 are presented the XRD phase analysis results. The same reactions could be expected to take place also in cracks and pores, but in smaller volume. These results suggest that the strengthening in phosphate seals result from two different mechanisms, chemical bonding mechanism due to chemical reaction between the coating material and the sealant, they also indicate the adhesive binding mechanism due to the formation of condensed aluminum phosphate in the structural defects of the coating.

The sealing of ZrO<sub>2</sub>-MgO by Aluminum phosphate may be given as the following equation:



**Microstructure investigation for Q-switched ND-YAG sealed ZrO<sub>2</sub>-MgO coatings:** Resistance to thermal cycling and the differential expansion coefficients of substrate and coating can to some extent be accommodated by porosity and micro-croaking in the spray layer. However, it is desirable to seal the surface to reduce or eliminate ingress of corrosive gases and fluids. Such sealing has been examined

using pulsed laser sealing can offer short wavelengths and short pulse durations which allow efficient energy coupling at low reflectance and a shallow influenced zone only a few microns deep. Pulsed frequencies and traverse speeds were varied and, as with the other processes, optimized first by metallographic examination.

X-ray analysis was used for the comparison of X-ray diffraction results (phase identification and quantitative phase analysis) of as sprayed coatings before and after the laser treatment as indicated in Figure 10 and Table 9. The X-ray diffraction results shows that the as sprayed coating after the laser treatment increases the crystallinity and no amorphous phase is present any more. So, the high strength and high toughness of zirconia stabilized with magnesia arise due to the presence of the tetragonal grains in the polycrystalline bodies.

The microstructure of the Q-switched Nd-YAG pulsed laser sealed ZrO<sub>2</sub>-MgO top coat in a few microns deep were investigated by SEM, Figure 11. This investigation clarified the process of laser sealing penetration into the coating as yielded a better understanding of surface improvement. The sealed top coat in a few microns (50 μm-100 μm) were highly densified, grain refined except for some closed pores formed in the laser sealing process. The total porosity of the laser sealed layer was lowered by 90%.

### Mechanical investigation

Mechanical properties were characterized in micro-hardness measurements and wear resistance measurements.

**Micro-hardness results:** Coating micro-hardness increased from 190 HV3 to 228 HV3 due to phosphate sealing. And coating micro-hardness increased from 190 HV3 to 342 HV3 due to laser sealing. The increasing of micro-hardness of the phosphate sealed coating can be

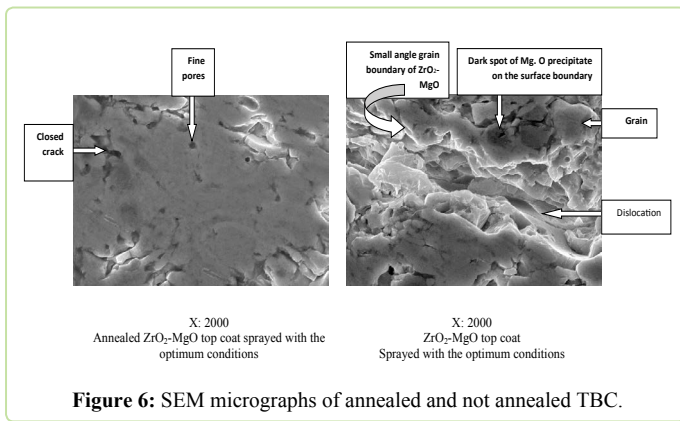


Figure 6: SEM micrographs of annealed and not annealed TBC.

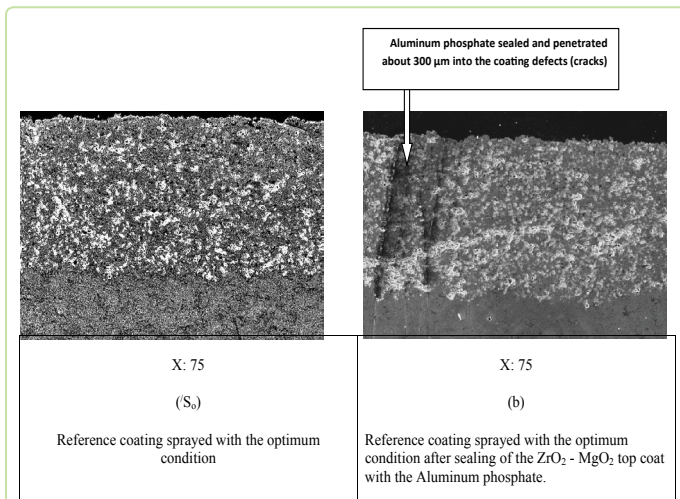


Figure 7: Optical micrographs of the reference and the modified Al PO<sub>4</sub> sealed coatings.

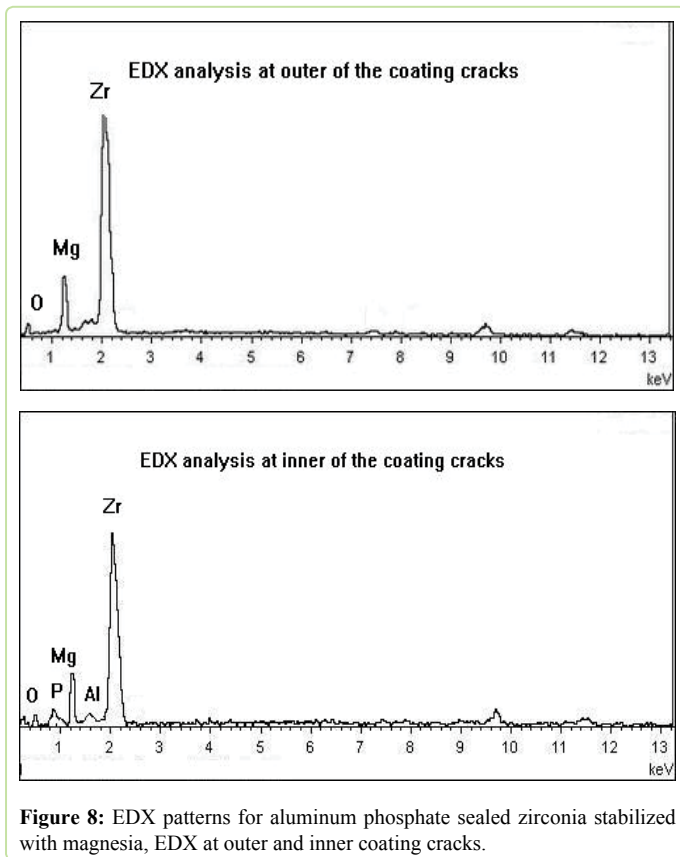


Figure 8: EDX patterns for aluminum phosphate sealed zirconia stabilized with magnesia, EDX at outer and inner coating cracks.

explained by improved bonding of the lamellar structure due to Aluminum phosphate sealant. In the melt layer (50 μm to 100 μm) of the laser sealing coatings were close to that of bulk ceramic, so there no weak points such as pores, micro-cracks or splat boundaries to lower the micro-hardness.

**Friction and wear resistance results:** Wear tests were performed only for ZrO<sub>2</sub>-MgO top coat. The hardness and abrasion resistance are increased due to phosphate (or laser) sealing.

The results of the abrasion tests were in line with the erosion resistance test results. Phosphate sealed coating showed excellent wear resistance, 80% lower weight losses than in reference coating. However, in this test the laser sealed ZrO<sub>2</sub>-MgO coating was even more abrasion resistant than the phosphate sealed coating; only a minor part of the melted top- layer was worn away. Figure 12 is illustrated the micrographs of the erosion wear trace in reference and sealed ZrO<sub>2</sub>-MgO (top coat) coating.

**Modified corrosion resistance and corresponding Vickers hardness investigations:** The electromagnetic parameters derived from linear polarization on experiment and the corresponding Vickers hardness for blank, reference, and modified specimens with the same spray conditions are present in Table 10.

The highest Vickers hardness and efficiency of thermal plasma spray coating protection under the laser sealed ZrO<sub>2</sub>-MgO of the modified coating conditions, amounts to 247 HV<sub>3</sub> and 99.5 %. However, the hardness and efficiency depend on the applied laser sealing due to the sealed top coat in a few microns were highly densities, grains refined with some closed pores formed in the laser sealing process. The corrosion rate of the Ni-base super alloy substrate was largely decreased through plasma spray coating protection under the laser sealed ZrO<sub>2</sub>-MgO coating.

**Thermal expansion and thermal cycling improvement:** Thermal expansion is the commonest source of mismatch strains, especially important TBC. The measured TEC of Ni-substrate is about 18 × 10<sup>-6</sup> K<sup>-1</sup> and nickel aluminum bond coat is about 14.9 × 10<sup>-6</sup> K<sup>-1</sup>. A mixed of oxide / metallic layer (ceramic with alloy) composed of combination 65 wt % ZrO<sub>2</sub>-MgO (65 wt % AMDRY 333 powder which used for top coat) with 35 wt % Ni-Al (35 wt % AMDRY 956 powder which used for bond coat) which they are corresponding to AMDRY 341 that air plasma thermally sprayed on the previous under layer ( bond coat ) to lower the difference of TEC of Ni-Al bond coat (14.9 × 10<sup>-6</sup> K<sup>-1</sup>) and TEC of ZrO<sub>2</sub>-MgO top coat (9.5 × 10<sup>-6</sup> K<sup>-1</sup>). Since, the mixing of oxide / metallic layer is selected for lowering the number of welding points at the contact between it and the under-layer bond coat where the heat is become transferred in a difficult way to provide excellent TBC (i.e. lower thermal conductivity) and excellent oxidation reaction as well as anchoring function to enhance the adhesion of the applied ZrO<sub>2</sub>-MgO top coat. The measured TEC of the mixed of ceramic with alloy was about 12 × 10<sup>-6</sup> K<sup>-1</sup> which close to that of bond coat and top coat, this leads to reduce the generation of residual stresses.

TBC has performed creditable in thermal cycle tests.

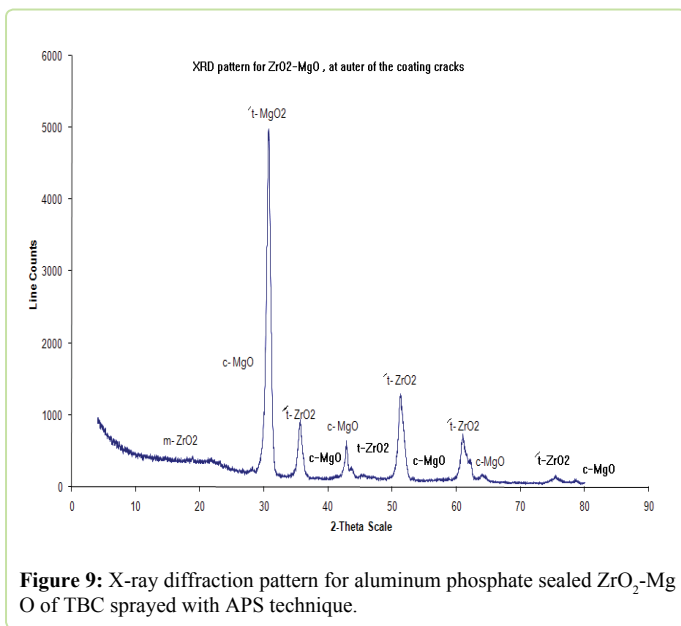


**Figure 9:** X-ray diffraction pattern for aluminum phosphate sealed ZrO<sub>2</sub>-MgO of TBC sprayed with APS technique.

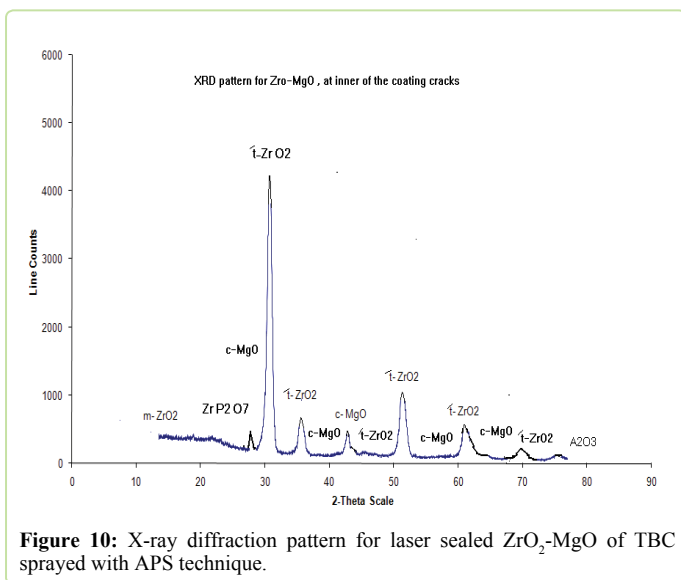


**Figure 10:** X-ray diffraction pattern for laser sealed ZrO<sub>2</sub>-MgO of TBC sprayed with APS technique.

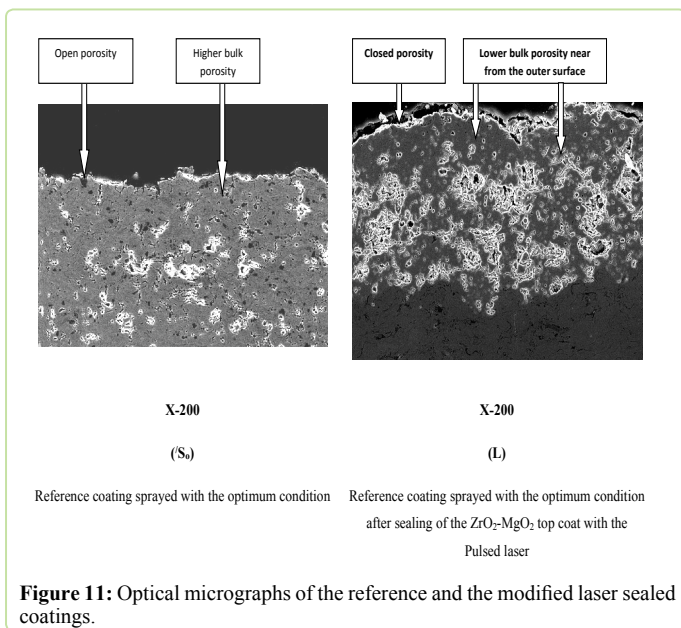


**Figure 11:** Optical micrographs of the reference and the modified laser sealed coatings.

Coating failure by thermal cycles depends on the applied stress on it and the strength of the substrate adhesion and inter-linking to the coating. A “Carousel” (or a Rolls-Royce) thermal cycling test on several coating systems was used, in which the maximum temperature was fixed at 1200°C for 20 second and forced cooling to 250°C for 20 second. In the test type used here the coating failure resulted from the stress generated by high temperature gradients in heating and cooling steps. On that basis it was easier to compare the pure thermal cycling resistance and strain tolerance properties of each modified TBC structure. Four specimens of each type were tested and the number of cycles to exfoliation was corded for each specimen.

Among the key parameters allowing to achieve the best thermo-mechanical properties (one of the APS coatings was showed no visible delaminating or cracking after 500 cycles) of the modified TBC are the optimum parameters which give the best molten state of the particles control of the coatings during spraying, using of stabilized zirconia resistance to destabilization with the thermal cycling of the TBC, during service, using NTA process on the surface of specimens to achieve high bond strength, the APS bond coat was diffusion heat-treated for 2 h at 1150°C and for 24 h at 800°C to achieve the best bond strength, mixing of oxide / metallic of TEC value in closed to the bond coat and top coat which was annealed at 800°C for 4 hours to increase the Young’s modulus (E) from 91 G pa to 135 G pa. This for enhance the adhesion of the applied stabilized zirconia (ZrO<sub>2</sub>-MgO) top coat and to reduce the generation of residual stress during thermal cycle test, and laser (or Aluminum phosphate) sealed ZrO<sub>2</sub>-MgO (top coat) coating. Some microstructure change took place in the coatings during the test series. Optical microstructure (SEM) of un-treated coating and treated coatings after different cycles are presented in Figure 13 A-J.

Reference coating (i.e. TBC sprayed with the optimum conditions and not modified) was showed a horizontal and vertical crack after 400 cycles indicate that the coating delamination process had already started. A horizontal crack

slightly above the bond coat was occurred after 500 cycles indicate that the large differences of TEC volume between the bond coat and top coat and increase the generation of residual stress during thermal cyclic test. A pure zirconia (non-stabilized zirconia) coating was damage after 280 cycles showed visible de-lamination and cracking.

Modified TBC was laser (or aluminum phosphate) sealed ZrO<sub>2</sub>-MgO top coat was showed excellent performance in the test and resisted more than 500 cycles. The coating peeled of near the bond coat after 950 cycles. In all phosphate sealed modified TBC, the failure occurred in the same mode and nearly half of the coating area was delaminated from the edge of the specimen in the form of a sickle. In these cases, the coating was failure within the ceramic layer in such way that the thickness of delaminated layer was higher in the specimen edges. So, it is possible that the delamination of the phosphate sealed coating occurred at the depth corresponding to sealant penetration. In laser sealed modified coatings, the failure occurred in the same mode and only the segments outside the laser-glazed track, were

**Table 9:** The quantitative XRD phase analysis results before and after laser sealed ZrO<sub>2</sub>-MgO top coat.

Position of analysis	m-ZrO <sub>2</sub> (w.t) %	t-ZrO <sub>2</sub> (w.t) %	c-Mg O (w.t) %
XRD analysis before laser treatment	0.08	78.12	21.8
XRD analysis after laser treatment	0.02	78.18	21.8

**Table 10:** The electromechanically parameters. Corrosion potential E<sub>corr</sub>, corrosion current I<sub>corr</sub>, polarization resistance R<sub>p</sub> and corrosion rate C<sub>R</sub> derived from linear polarization experiments and the corresponding hardness (HV<sub>3</sub>) for blank specimen, reference and modified coatings with the same spray conditions.

Specimen Type	E <sub>corr</sub> (v)	R <sub>p</sub> (Ohm. cm <sup>2</sup> ±10 <sup>3</sup> )	I <sub>corr</sub> (μ. A/Cm <sup>2</sup> )	CR (m. p. y)	Efficiency (%)	Hardness (HV <sub>3</sub> )
Ni-base super alloy substrate	-0.297	8.416	3.2906	0.97832	—	180
ZrO <sub>2</sub> -MgO reference coating	-0.237	185.8	0.22988	0.06834	93.01	200
Aluminum- Phosphate sealed ZrO <sub>2</sub> -MgO Modified coating	-0.318	83.3	0.1802	0.053	94.5	200
Laser - sealed ZrO <sub>2</sub> -MgO modified coating	-0.165	2899	0.01678	0.004	99.5	247

**Table 11:** Calculated thermal conductivity, λ (T) results for reference material and modified coatings corresponding to the measured porosity.

Coating layer type deposited on Ni- substrate by using APS technique	Porosity δ (%)	Density ρ (Kg/m <sup>3</sup> )	Specific heat Cp (J/Kg/K)	Thermal diffusivity α (* 10 <sup>-7</sup> m <sup>2</sup> /S)	Thermal conductivity λ = ρ. C <sub>p</sub> α (W/m. K)	Temperature (°C)
Ni-base-super alloy DIN (2.4631)	0.1	8900	444	190	75	27
			580	130	66	300
			635	150	84.7	700
			647	160	92.1	1200
Ni-5wt % Al bond coat	2	7500	450	40	9	27
			530	41.5	10.2	300
			560	43	13	700
			585	34	15	1200
ZrO <sub>2</sub> -20 wt% MgO	9.8	4280	614	2.85	0.75	27
			640	7.5	2	300
			657	7.8	2.2	700
			660	8.85	2.5	1200
Aluminum phosphate sealed ZrO <sub>2</sub> -20 wt% MgO top coat (modified coating)	2.9	4380	625	4.3	1.2	27
			675	9.1	2.7	300
			680	10.4	3.1	700
			684	12.7	3.8	1200
Laser sealed ZrO <sub>2</sub> -20 wt% MgO top coat (modified coating)	3.9	4350	634	2.9	0.8	27
			650	7.4	2.1	300
			655	8.4	2.4	700
			667	8.7	2.55	1200

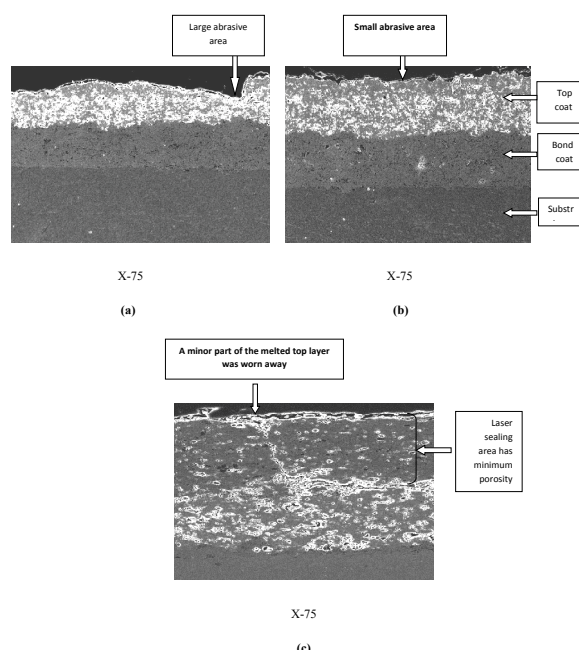
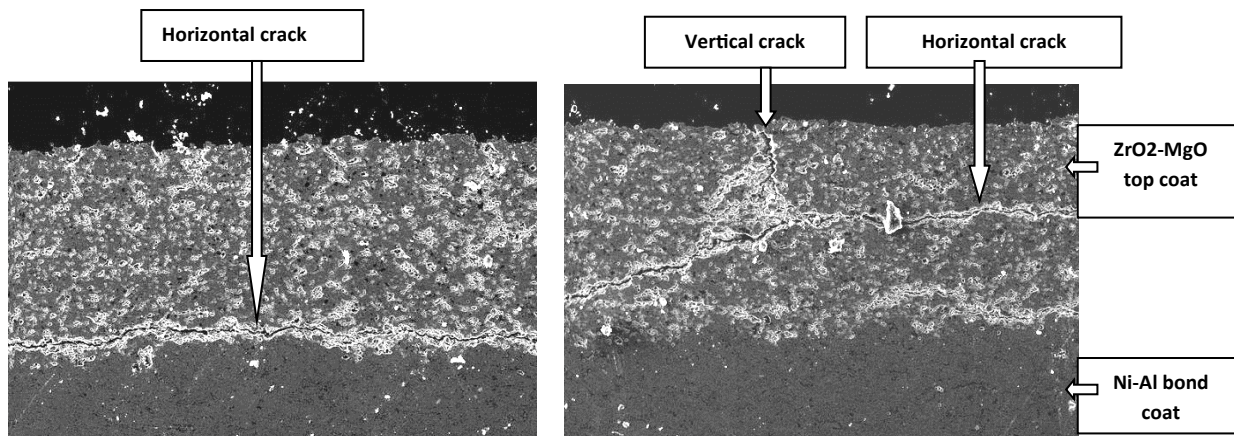


**Figure 12:** SEM micrographs of the erosion wear traces in (a) reference coating, (b) Aluminum phosphate and (c) laser sealed ZrO<sub>2</sub>-MgO coating.

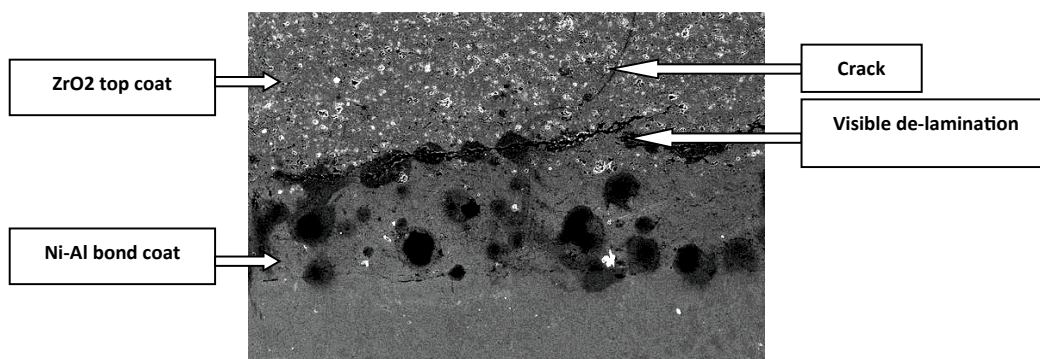


X-75

Figure 13 A: Reference coating after 500 cycles

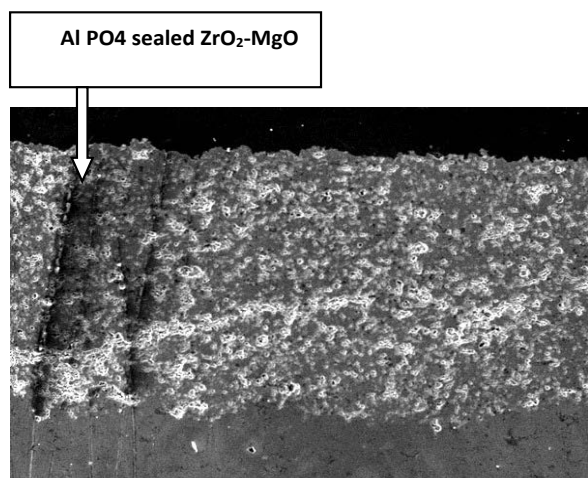
X-75

Figure 13 B: Reference coating after 400 cycle.



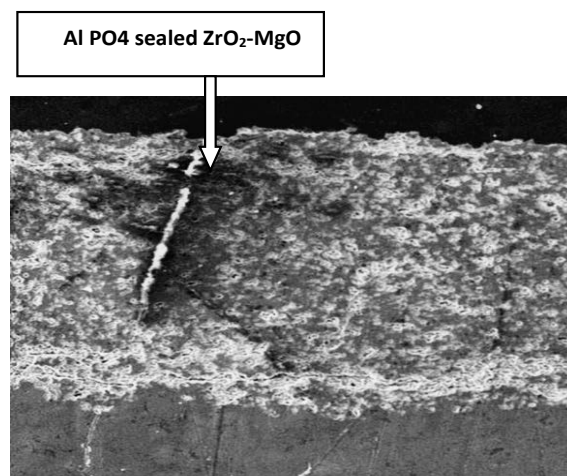
X-75

Figure 13 C: Non-stabilized ZrO<sub>2</sub> (pure zirconia) after 280 cycles.



X-75

Figure 13 D: Al PO<sub>4</sub> sealed ZrO<sub>2</sub>-MgO.



X-75

Figure 13 E: Al PO<sub>4</sub> sealed ZrO<sub>2</sub>-MgO after 500 cycles.

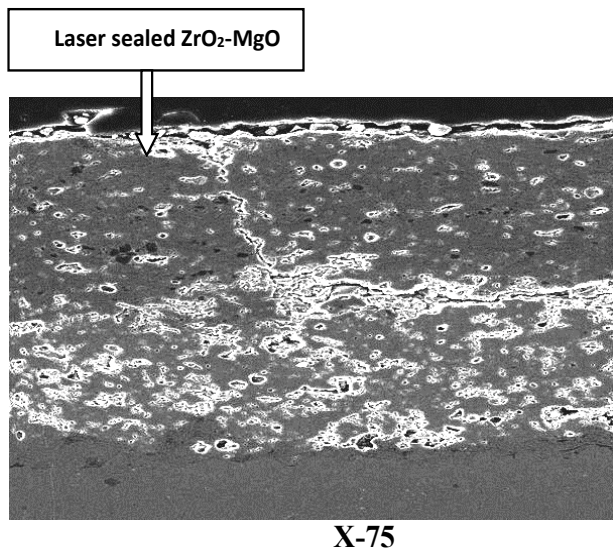


Figure 13 F: Laser sealed ZrO<sub>2</sub>-MgO before thermal cyclic test.

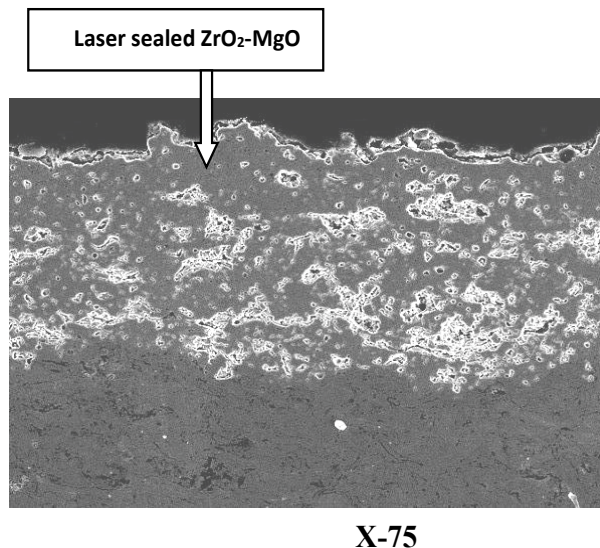


Figure 13 G: Laser sealed ZrO<sub>2</sub>-MgO after 500 cycles.

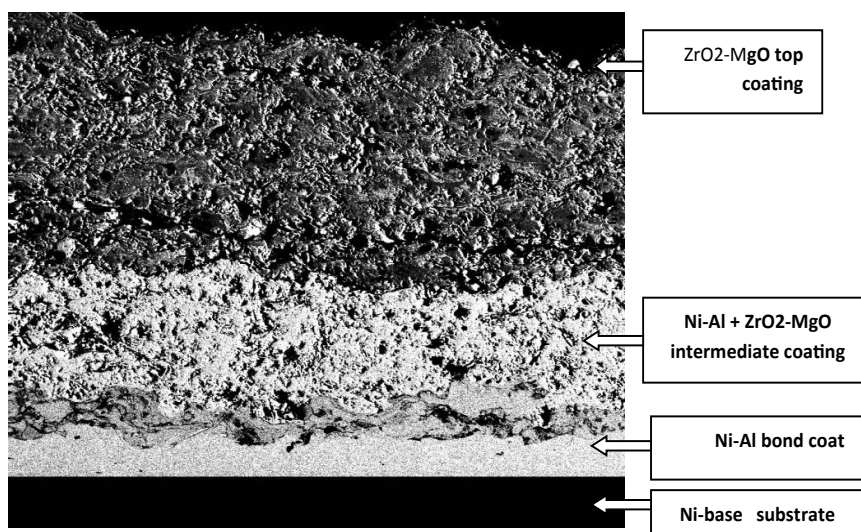


Figure 13 H: Triple coating after 500 cycles.

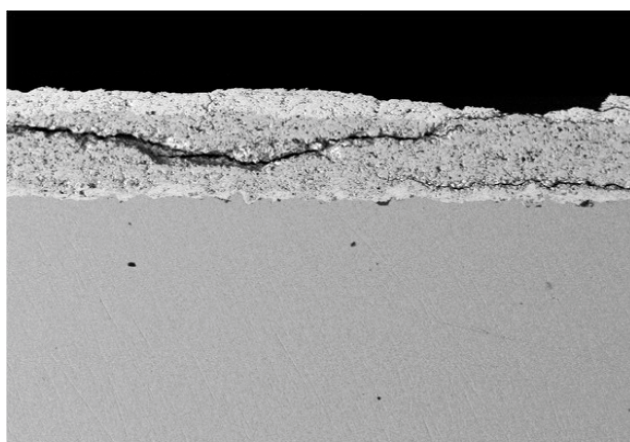
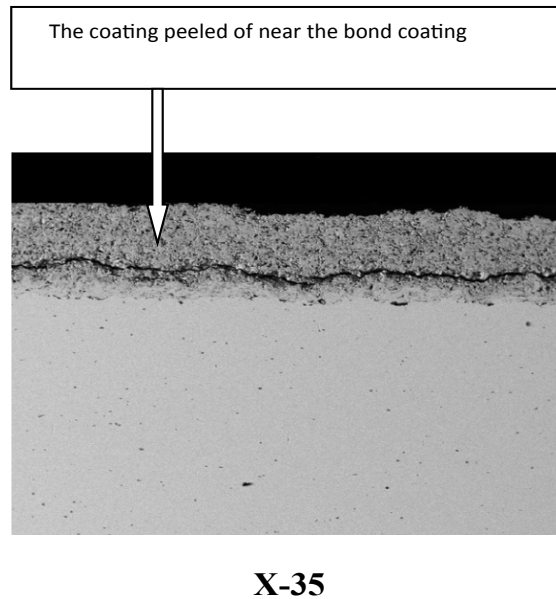


Figure 13 I: Modified triple coating of Al PO<sub>4</sub> sealed ZrO<sub>2</sub>-MgO after 950 cycles.



**Figure 13 J:** Modified triple coating of laser sealed ZrO<sub>2</sub>-MgO after 950 cycles.

peeled off and the laser, glazed area remained unaffected, but at some point, the whole coating was peeled of near the bond coat.

It can be assumed that the segmentation cracked, and laser-sealed coating structure tolerates better tensile stresses as compressive stresses. Under tensile load the coating cracks can be opened, but in compression that not possible. However, the stress situation is not so simple in practice, because there should always be a temperature gradient in TBC. A stress gradient is induced into the coating. The stress gradient creates bending stresses that still increase the effect of crack initiation and growth at weak points of the coating such as the edge regions of the coating and the TBC/bond coat interface. The advantage of a segmentation cracked, and laser-sealed coating is that tensile and bending stresses not directly, accumulate into a coating in macro-scale as they do in the case of normally (reference) structured APS of TBC.

Thermal cycling resistance was dramatically deteriorated due to aluminum phosphate sealing. The failure mode of the aluminum phosphate sealed coatings. These coatings were not delaminated regularly at the bond coat interface but were fractured within the ceramic layer in the form of circle. These fractured coating pieces were thicker at the specimen edge side referring to irregular local sealant penetration and coating densification.

**Thermal conductivity investigation:** Calculated thermal conductivity  $\lambda$  (T) results of two successive measurement cycles ( $C_p$  (T),  $\alpha$  (T),  $\rho$ ) are present in Table 11. The temperature (T), specific heat  $C_p$  (T), and the density  $\rho$  data for each type of reference material was used in the thermal conductivity at certain temperature  $\lambda$  (T) calculations also for treated (modified) coatings.

The modification processes had effect on thermal conductivity of TBC [22,23]. Phosphate sealing significantly increased thermal conductivity due to sealant filling the

cracks and pores. In the case of aluminum phosphate sealed ZrO<sub>2</sub>-MgO modified coatings, the aluminum phosphate increased thermal conductivity. The effect of laser sealed ZrO<sub>2</sub>-MgO modified coatings; the dense laser sealing top layer slightly increased thermal conductivity. This slightly difference can be explained by the fact that the macro-cracks are not present in the laser sealed region and there is not precipitation of Mg O during laser sealing effect, leading to stabilization of tetragonal zirconia prevented the formation meta-zirconia, by 90 % in a few microns which were highly densities, grain refined except for some closed pores formed in the laser sealing process. Thermal conductivity of the sintered tetragonal sometime called (tetragonal zirconia poly-crystals-TZP). Thermal conductivity of the zirconia stabilized with yttria has been reported by Stevens to be equal at 200 0C to 2.9 w/(mk) [24].

The control of the upper and lower limits has been shown as influential on the materials performance. The increase of the upper size limits of the sprayed powder produces more porous coatings of low thermal conductivity due the poor inter-lamellar contacts between the grains.

## Conclusions

Several new coating methods have evolved, and older methods were refined. New analytical tools are introduced. The development and evaluation of coatings are expensive and there is now a need, more than ever, to conserve resources, optimize test programmed and for a greater coordination dissemination of information.

In this study, The TBC system was investigated using several processes to conclude the influence of plasma spray parameters on the coating performance and to conclude the advanced processing approaches for producing TBC of high quality performance, from the obtained data, discussion and interpretation of the results, it could be concluded that:

1. The corrosion resistance properties of Ni-base

super alloy substrate are enhanced significantly by thermal spray treatment.

2. The close thermal expansion values matched between the substrate & bond coat, matched between the bond coat & intermediate coat and matched between the intermediate coat & top coat which led to significantly longer thermal barrier substrate in cycling temperature tests. Since these layers were selected for lowering the number of welding points at the contact layers between them where the heat is become transferred in a difficult way to provide excellent TBC (i.e. lower thermal conductivity) and excellent oxidation reaction as well as anchoring function to enhance the adhesion of the applied top coat.

3. The work performed has been devoted to a better understanding of the importance of coating temperature control during plasma spraying of thermal barrier plasma torch working conditions as well as powder have been the following:

- The cooling of deposit with air jets blowing orthogonally to the plasma jet or onto the substrate surface.

- The relative movements of the torch-substrate controlling the deposited strands and their overlapping (resulting in passes thickness).

- It is better; to obtain high micro-hardness to spray with a high torch linear velocity to have thin deposition passes (adjusted by controlling the substrate rotating velocity).

- The results seem to show that all the investigated parameters are linked to adhesion between lamellae and cracks network (induced by stresses relaxation, stresses due to spraying conditions and coating cooling).

4. The introducing (65 wt.%  $ZrO_2$ -Mg O plus 35 wt. % Ni-Al) composite coating between the Ni-Al bond coat and  $ZrO_2$ -MgO top coat led to obtain a TBC shows dense microstructure, uniformly particles, as well as very few micro-structure defects.

5. Reducing heat losses increases efficiency but raises temperatures. Thus, thermal barrier coatings are needed on valves, piston crowns and cylinder heads. The adiabatic engine, requiring TBC such as zirconia stabilized with magnesia on a Ni-Al bond coating, graded and up to 0.8mm thick has performed well on piston crowns of marine diesels using normal fuel. Low quality fuel contains vanadium (V) which reacts with  $Y_2O_3$  or CaO stabilizers in the  $ZrO_2$  and causes disintegration. Since, Mg O stabilizer is more resistant.

6. The penetration of aluminum phosphate sealed into the (zirconia stabilized with magnesia top) coatings near the surface is accompanied with two different mechanisms, chemical bonding (due to chemical reaction between the coating material and the sealant) and adhesion binding (due to the formation of condensed aluminum phosphate in the structural defects of the coating).

The laser sealed zirconia stabilized with magnesia (top coat) is accompanied with grain refining and transformation hardening a coating surface without affecting the bulk of the

coat itself and with no phase transition present due to the localized nature of laser heating.

## References

1. Swadźba L, Moskal G, Mendala B, Hetmańczyk M (2008) Characterization of microstructure and properties of TBC systems with gradient of chemical composition and porosity. Arch Metall Mater. 53: 945-954.
2. Moskal G, Swadźba L, Mendala B, Góral M, Hetmańczyk M (2010) Degradation of the TBC system during the static oxidation test. J Microsc Oxford. 237: 450-455.
3. Antou G, Montavon G, Hlawka F, Cornet A, Coddet C, et al. (2006) Modification of thermal barrier coating architecture by in situ laser remelting. J Eur Ceram Soc. 26: 3583-3597.
4. Petorak C, Ilavsky J, Wang H, Porter W, Trice R (2010) Microstructural evolution of 7 wt%  $Y_2O_3$ - $ZrO_2$  thermal barrier coatings due to stress relaxation at elevated temperatures and the concomitant changes in thermal conductivity. Surf Coat Technol. 205: 57-65.
5. Renteria AF, Saruhan B, Schulz U, Raetzer-Scheibe HJ, Haug J, et al. (2006) Effect of morphology on thermal conductivity of EB-PVD PYSZ TBC's. Surf Coat Technol. 201: 2611-2620.
6. Schafrik R and Sprague R (2004) Saga of Gas Turbine Materials: Part III. Advanced Materials and Processes, 01 May 2004.
7. Pauschitz A, Roy M, Franek F (2008) Mechanisms of sliding wear of metals and alloys at elevated temperature. Tribology International. 41: 584-602.
8. Yoshihisa J, Yokoyama F, Yamasaki T, Ohmae N (2010) The tribological characteristics of Ni-Cr cast alloy at 1000 degree C in air. Tribology Online. 5: 27-32.
9. Hatab AK, Bukhaiti AM, Krupp U, Kanthem M (2011) Cyclic Oxidation Behavior of IN 718 Superalloy in Air at High Temperatures. Oxidation of Metals. 75: 209-228.
10. Osorio JD, Hernandez-Ortiz JP, Toro A (2014) Microstructure characterization of thermal barrier coating systems after controlled exposure to a high temperature. Ceramics International. 40: 4663-4671.
11. Erdem M and Turker M (2012) High temperature oxidation behaviour of a Ni based superalloy produced by mechanical alloying. Scientific Research and Essays. 7: 4123-4129.
12. Wang M (2009) MCrAlY of IN 100 and heat treated at 950 at 1050 deg. C in a vacuum atmosphere for 2 hours exhibits the parabolic oxidation behaviour. Surface and Coatings. 203: 2186-2192.
13. DeFlora MG and Pellizari M (2009) Behavior at elevated temperature of 55NiCrMoV7 tool steel. Material and Manufacturing Processes. 24: 791-795.
14. Fernandes F, Ramalho A, Loureiro A, Guilemany JM, Torrell M, et al. (2013) Influence of nanostructured ZrO2 additions on wear resistance of Ni-based alloy coatings

- deposited by APS process. *Wear*. 303: 591-601.
15. Petorak C, Ilavsky J, Wang H, Porter W, T r i c e R (2010) Microstructural evolution of 7 wt%  $Y_2O_3$ - $ZrO_2$  thermal barrier coatings due to stress relaxation at elevated temperatures and the concomitant changes in thermal conductivity. *Surf Coat Technol*. 205: 57-65.
  16. Parker WJ, Jenkins RJ, Butler CP, Abbott GL (2004) Flash method of determining thermal diffusivity, heat capacity and thermal conductivity. *J Appl Phys*. 32: 1679.
  17. Rutkowski P, Stobierski L, Górny G (2014) Thermal stability and conductivity of hot-pressed  $Si_3N_4$ -graphene composites. *J Therm Anal Calorim*. 116: 321-328.
  18. Kövér M, Behúlová M, Drienovský M, Motyčka P (2015) Determination of the specific heat using laser flash apparatus. *J Therm Anal Calorim*. 122: 151-156.
  19. Rutkowski P, Klimczyk P, Jaworska L, Stobierski L, Dubiel A (2015) Thermal properties of pressure sintered alumina-graphene composites. *J Therm Anal Calorim*. 122: 105-114.
  20. Niemiec D, Moskal G, Mikuškiewicz M, Mościcki A, Kałamarz P, et al. (2014) Influence of top-surface condition on oxidation resistance of NiCrAlY coating on Inconel 625 alloy. *Ochr Przed Kor*. 7: 255-266.
  21. Moskal G, and Niemiec D (2015) Influence of surface condition on oxides layer morphology on NiCrAlY coating during oxidation at temperature 1000°C and 1100°C. *Solid State Phenom*. 227: 385-388.
  22. Moskal G (2009) Thermal barrier coatings: characteristics of microstructure and properties, generation and directions of development of bond. *J Achiev Mater Manuf Eng*. 37: 323-331.
  23. Moskal G (2013) Microstructural characterization of Ni(Co)CrAlY powders designed for thermal spraying of bondcoat for TBC systems. *Solid State Phenom*. 203-204:435-438.
  24. Ratzler-Scheibe HJ, Schulz U, Krell T (2006) The effect of coating thickness on the thermal conductivity of EB-PVD PYSZ thermal barrier coatings. *Surf Coat Technol*. 200: 5636-5644.